Siberian Branch of Russian Academy of Science

BUDKER INSTITUTE OF NUCLEAR PHYSICS

R.R. Akhmetshin, V.M. Aulchenko, V.Sh. Banzarov,
L.M. Barkov, N.S. Bashtovoy, A.E. Bondar,
D.V. Bondarev, A.V. Bragin, S.K. Dhawan
S.I. Eidelman, D.A. Epifanov, G.V. Fedotovich
N.I. Gabyshev, D.A. Gorbachev, A.A. Grebeniuk,
D.N. Grigoriev, F.V. Ignatov, S.V. Karpov,
V.F. Kazanin, B.I. Khazin, I.A. Koop,
P.P. Krokovny, A.S. Kuzmin, I.B. Logashenko,
P.A. Lukin, A.P. Lysenko, K.Yu. Mikhailov,
A.I. Milstein, I. N. Nesterenko, M.A. Nikulin,
V.S. Okhapkin, A.V. Otboev, E.A. Perevedentsev,
A.A. Polunin, A.S. Popov, S.I. Redin,
B.L. Roberts, N.I. Root, A.A. Ruban,
N.M. Ryskulov, A.G. Shamov, Yu.M. Shatunov,
B.A. Shwartz, A.L. Sibidanov, V.A. Sidorov,
A.N. Skrinsky, V.P. Smakhtin, I.G. Snopkov,
E.P. Solodov, A.A. Valishev, Yu.V. Yudin,
A.S. Zaitsev, S.G. Zverev

STUDY OF $\phi \to \pi^+\pi^-\pi^0$ WITH CMD-2 DETECTOR

Budker INP 2006-28

Novosibirsk
2006

Study of $\phi \to \pi^+\pi^-\pi^0$ with CMD-2 detector

R.R. Akhmetshin[a], V.M. Aulchenko[a,b], V.Sh. Banzarov[a], L.M. Barkov[a,b], N.S. Bashtovoy[a], A.E. Bondar[a], D.V. Bondarev[a,b], A.V. Bragin[a], S.K. Dhawan[d], S.I. Eidelman[a,b], D.A. Epifanov[a], G.V. Fedotovich[a,b], N.I. Gabyshev[a], D.A. Gorbachev[a], A.A. Grebeniuk[a], D.N. Grigoriev[a,b], F.V. Ignatov[a], S.V. Karpov[a], V.F. Kazanin[a,b], B.I. Khazin[a,b], I.A. Koop[a,b], P.P. Krokovny[a,b], A.S. Kuzmin[a,b], I.B. Logashenko[a,c], P.A. Lukin[a], A.P. Lysenko[a], K.Yu. Mikhailov[a], A.I. Milstein[a,b], I. N. Nesterenko[a,b], M.A. Nikulin[a,b], V.S. Okhapkin[a], A.V. Otboev[a], E.A. Perevedentsev[a,b], A.A. Polunin[a], A.S. Popov[a], S.I. Redin[a], B.L. Roberts[c], N.I. Root[a], A.A. Ruban[a], N.M. Ryskulov[a], A.G. Shamov[a], Yu.M. Shatunov[a], B.A. Shwartz[a,b], A.L. Sibidanov[a], V.A. Sidorov[a], A.N. Skrinsky[a], V.P. Smakhtin[f], I.G. Snopkov[a], E.P. Solodov[a,b], A.A. Valishev[a], Yu.V. Yudin[a], A.S. Zaitsev[a,b], S.G. Zverev[a]

CMD-2 Collaboration

[a] *Budker Institute of Nuclear Physics, Russian Acad. Sci. 630090, Novosibirsk, SB RAS*
[b] *Novosibirsk State University, 630090, Novosibirsk, Russia*
[c] *Boston University, Boston, MA 02215, USA*
[d] *Yale University, New Haven, CT 06511, USA*
[e] *University of Pittsburgh, Pittsburgh, PA 15260, USA*
[f] *Weizmann Institute of Science, 76100, Rehovot, Israel*

Abstract

The cross section of the process $e^+e^- \to \pi^+\pi^-\pi^0$ has been measured in the c.m. energy range 984–1060 MeV with the CMD-2 detector at the VEPP-2M collider at BINP. The obtained value of $Br(\phi \to e^+e^-)Br(\phi \to \pi^+\pi^-\pi^0) = (4.51 \pm 0.16 \pm 0.11) \times 10^{-5}$ is in good agreement with the previous measurements and has the best accuracy. The analysis of the Dalitz plot was performed. The contributions of the dominant $\phi \to \rho\pi$ mechanism as well as small direct $\phi \to 3\pi$ production amplitude were determined.

1 Introduction

A study of e^+e^- annihilation into hadrons at low energies has a long history, but despite decades of experiments, new precise measurements are still interesting and can provide important information about interactions of light quarks and spectroscopy of their bound states.

This work is devoted to a study of the process $e^+e^- \to \pi^+\pi^-\pi^0$ within the ϕ-meson energy range with the CMD-2 detector [1, 2], at the VEPP-2M e^+e^- collider [3] in the Budker Institute of Nuclear Physics (Novosibirsk).

It was proposed long time ago by Gell-Man, Sharp and Wagner [4] that $\phi \to \pi^+\pi^-\pi^0$ decay proceeds via the $\rho\pi$ intermediate state. First evidence of $\rho\pi$ dominance was obtained in [5]. Later, experiments with CMD-2 and SND detectors [6, 7] confirmed this conclusion and set upper limits on the non-$\rho\pi$ amplitude. However, some phenomenological models, for example effective lagrangian approach [8, 9, 10], HLS [11] predicted contact term in this decay. Recently new results on $\phi \to \pi^+\pi^-\pi^0$ from the KLOE experiment [12] as well as preliminary results from the CMD-2 detector [13] were reported. The final results of the latter experiment is presented here.

The other important issue of this work is a precise measurement of the cross section $\sigma_{3\pi}(E)$ used in the calculation of the hadronic contribution to the muon anomalous magnetic moment $(g-2)_\mu$. The measurement of $\phi \to \pi^+\pi^-\pi^0$ branching ratio as well as parameters of $\phi - \omega$ mixing is also of large interest.

2 CMD-2 detector

The layout of CMD-2(cryogenic magnetic detector) is shown in Fig 1. This general-purpose detector combines features of a spectrometer for detection of charged particles with good calorimetry for photons.

The tracking part of the detector consists of a cylindrical drift chamber (DC) and double-layer multiwire proportional chamber (Z-chamber). Outside the superconducting solenoid with a 1 T magnetic field a barrel electromagnetic calorimeter based on CsI scintillation crystals and muon range system are placed. To keep good energy resolution of the barrel calorimeter

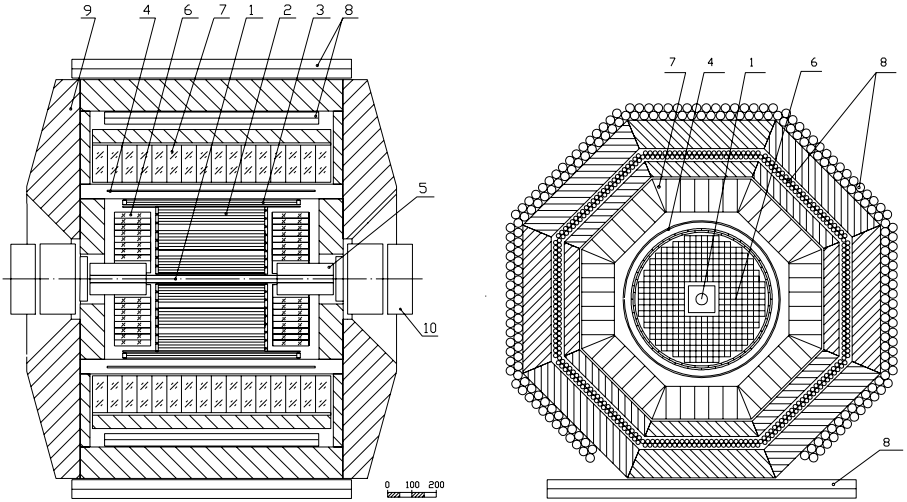

Figure 1: Layout of CMD-2. 1 – vacuum chamber; 2 – drift chamber(DC); 3 – Z-chamber(ZC); 4 – superconducting solenoid; 5 – compensating solenoid; 6 – BGO endcap calorimeter; 7 – CsI barrel calorimeter; 8 – muon range system; 9 – iron yoke; 10 – quadrupole lenses.

the solenoid design was optimized to have a small thickness, 0.38 X_0. The endcap calorimeter is made of BGO scintillation crystals. Both barrel and endcap calorimeters cover a solid angle of $0.92\times4\pi$ steradians.

This analysis of $e^+e^- \to \pi^+\pi^-\pi^0$ reaction is based on the experimental information collected at the CMD-2 detector in 1997-1998 (PHI98 statistics) with integrated luminosity of about 12 pb^{-1}.

The data were collected at 54 points in the center-of-mass energy range from 984 to 1060 MeV.

3 Selection of $\pi^+\pi^-\pi^0$ events

3.1 Selection criteria

The cross section measurement as well as Dalitz plot studies were based on fully reconstructed 3π events. Partially reconstructed events were used to determine corrections to the detection efficiency.

The main data sample contains events with two charged particles (one positive and one negative) and two or more reconstructed photon clusters,

selected by following criteria ($\mathbf{2T}\pi^0$ – 2 tracks and 1 π^0):

All charged particles are required to hit detector within the solid angle limited by the polar angle $|\pi/2-\theta| < 0.67$ radians to provide high efficiency track reconstruction both in Z-chamber and DC. The same criterian was applied to the polar angles of γ-quants to avoid edge effects for the detection efficiency in the CsI calorimeter. For charged particles:

- For each track the spread of the hits from the optimal helix in the $(R-\varphi)$ plane $\sigma_R < 0.1$ cm and in the $(R-Z)$ plane $\sigma_Z < 3$ cm (to be compared with the average spatial resolution of the DC: $\sigma_R < 0.025$ cm and $\sigma_Z < 0.4$ cm in the transverse and longitudinal directions)

- Tracks should be acollinear in the $(R-\varphi)$ projection $|\pi-|\varphi_2-\varphi_1|| > 0.1$ to reject Bhabha events and a space angle between tracks should be $0.1 < \psi < 3.0$ to reject events of γ conversion in the wall of the detector vacuum pipe

- The closest approach of each track to the beam axis should be $R_{\min} <$ 0.2 cm in the $(R-\varphi)$ projection while the distance from a track to the interaction point along the beam direction should be $|Z_{trk}| < 10$ cm

- The momentum of each track is required to be $P_\pi < 500$ MeV/c

- To reject events with initial state radiation (ISR) of a hard photon we apply the cut on the absolute value of 3π system total momentum $|\vec{P}_{\pi^+} + \vec{P}_{\pi^-} + \vec{P}_{\pi^0}| < 100$ MeV/c

- Charged particle energy loss per unit pathlength in the DC should be $dE/dx < 2(dE/dx)_{MIP}$ to suppress charged kaons

A neutral pion was identified by two photons with the energy of each one $E_\gamma > 30$ MeV and invariant mass in the range of 80 MeV/c^2 < M$_{\gamma\gamma}$ < 170 MeV/c^2.

If more than two photons were detected, we selected events, where only one π^0 candidate was found among all $\gamma\gamma$ combinations, $N_{\pi^0} = 1$.

Figure 2 shows the 2D distribution of the selected experimental events at $E_{beam} = 509.5$ MeV over charged particle momenta P_{π^+} versus P_{π^-}.

Clearly seen are events of three types: $\pi^+\pi^-\pi^0$ inside the allowed kinematic region; K_LK_S, where $K_S \to \pi^+\pi^-$along the calculated curve of $P_+(P_-)$ dependence; K^+K^-along two lines with P($K^\pm$)=107 MeV. The charged particles from the $K^\pm$ decay can have momenta in the large range up to the 310 MeV/c ($K^\pm \to \mu^\pm\nu_\mu$). Two lines show the location of the events with one kaon decaying to the lighter particles.

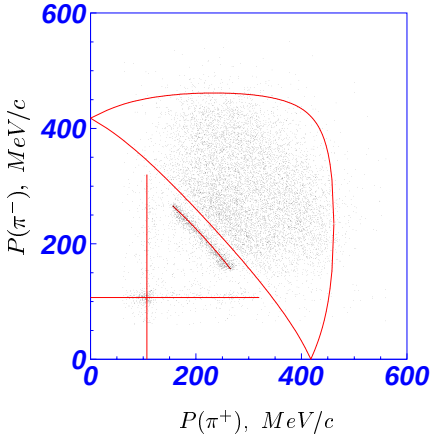

Figure 2: Distribution of experimental events on the P_+ $VS.$ P_- scatter plot. Also shown are: $\pi^+\pi^-\pi^0$ allowed kinematic region, calculated curve of $P_+(P_-)$ dependence for $K_LK_S$events and two lines with P($K^\pm$)=107 MeV, indicating location of K^+K^-events.

Finally we selected events above the lower boundary of the 3π allowed kinematic region to suppress events of $\phi \to K_SK_L$ decay, and applied a cut on the track momentum $P_\pi > 120$ MeV/c to reject events of $\phi \to K^+K^-$ decay.

With the above criteria, 104849 events were selected in the c.m. energy range $E_{CM} = \sqrt{s} = 984 \div 1060$ MeV, see Table 1.

3.2 Detection efficiency

The $\pi^+\pi^-\pi^0$ detection efficiency, $\varepsilon_{3\pi}^{MC}$, was determined from the full Monte Carlo simulation based on GEANT3 program [15]. It was calculated as:

$$\varepsilon_{3\pi}^{MC} = N^{sel}/N^{gen}, \tag{1}$$

where: N^{gen} – the number of generated 3π events, N^{sel} – the number of 3π events passed all selections.

The value of $\varepsilon_{3\pi}^{MC} = 4.71\pm0.02\%$ was obtained using a large MC sample of 10^6 generated $e^+e^- \to \pi^+\pi^-\pi^0$ events at the c.m. energy $\sqrt{s} = 1019.5$ MeV. The energy dependence of $\varepsilon_{3\pi}^{MC}$ is included in the efficiency correction, which is discussed in Section 4.

Table 1: Numbers of 3π events. First column – the number of the energy point, the second column – the number of the scan, E_{beam} – beam energy, N_{sel} – the number of selected ($2\mathrm{T}\pi^0$) 3π events, N_{bg} – the number of background events, $N_{3\pi} = N_{sel} - N_{bg}$

#	#scan	E_{beam}, MeV	N_{sel}	$N_{3\pi}$	N_{bg}
1	1	509.347 ± 0.016	560	533± 28	27±16
2	1	509.279 ± 0.028	162	162± 16	0± 8
3	1	492.010 ± 0.300	87	74± 11	13± 8
4	1	502.000 ± 0.300	148	101± 15	47±13
5	1	505.299 ± 0.060	374	319± 23	55±16
6	1	508.038 ± 0.012	849	810± 35	38±20
7	1	508.434 ± 0.011	2439	2439± 58	0±29
8	1	508.906 ± 0.011	1625	1574± 48	51±26
9	1	509.628 ± 0.017	2185	2115± 56	69±31
10	1	508.769 ± 0.007	3325	3325± 69	0±35
11	1	509.216 ± 0.008	1262	1260± 42	1±21
12	1	509.289 ± 0.004	4162	4066± 76	95±41
13	1	509.345 ± 0.010	1205	1149± 41	55±23
14	1	509.792 ± 0.006	2186	2183± 56	2±29
15	1	509.888 ± 0.008	3945	3941± 74	3±37
16	1	510.316 ± 0.007	3171	3095± 67	76±36
17	1	510.760 ± 0.010	1107	1101± 39	5±20
18	1	511.199 ± 0.008	986	977± 37	9±19
19	1	513.730 ± 0.032	318	277± 21	41±14
20	1	516.721 ± 0.100	118	106± 13	11± 7
21	1	519.782 ± 0.043	68	57± 10	10± 6
22	1	529.803 ± 0.072	79	25± 11	53±12
23	2	505.217 ± 0.060	350	331± 22	18±13
24	2	507.892 ± 0.012	1027	1000± 38	26±20
25	2	508.362 ± 0.007	2610	2547± 60	62±32
26	2	508.827 ± 0.004	5862	5794± 90	67±46
27	2	509.414 ± 0.005	10272	10226±119	45±60
28	2	509.929 ± 0.002	9810	9733±116	76±59
29	2	510.366 ± 0.070	4397	4343± 78	53±40
30	2	510.855 ± 0.050	1235	1203± 41	31±22
31	2	511.629 ± 0.011	971	924± 37	47±21
32	2	514.061 ± 0.018	273	235± 20	38±14
33	2	516.960 ± 0.028	123	109± 13	13± 8
34	2	519.875 ± 0.063	120	92± 13	28±10

35	2	525.046 ± 0.059	100	48± 12	51±12
36	3	502.000 ± 0.300	239	199± 19	40±13
37	3	492.000 ± 0.300	153	112± 15	40±12
38	3	502.000 ± 0.300	216	180± 19	35±13
39	3	505.020 ± 0.300	350	310± 23	39±16
40	3	507.756 ± 0.060	957	920± 37	37±21
41	3	508.406 ± 0.050	4176	4109± 76	67±40
42	3	508.878 ± 0.004	6906	6759± 99	147±53
43	3	509.415 ± 0.005	7478	7434±101	44±51
44	3	509.774 ± 0.006	7691	7691±103	0±51
45	3	510.244 ± 0.005	4758	4647± 82	111±44
46	3	510.707 ± 0.007	1662	1583± 49	78±28
47	3	511.258 ± 0.017	893	821± 36	72±22
48	3	513.735 ± 0.020	342	317± 22	24±13
49	3	516.691 ± 0.026	195	147± 17	48±13
50	3	519.708 ± 0.043	82	42± 11	39±11
51	3	524.617 ± 0.061	56	37± 9	19± 7
52	3	529.503 ± 0.080	20	20± 6	0± 4
53	3	508.521 ± 0.040	921	894± 36	27±19
54	3	510.035 ± 0.040	243	243± 19	0±10

Figures 3,4,5,6,7,8 demonstrate the comparison of distibutions for MC simulated events and for experimental data (selected at the ϕ meson peak, where background is small) over some selection parameters.

All experimental distributions except $M_{\gamma\gamma}$ are in reasonable agreement with Monte Carlo.

The $\gamma\gamma$ invariant mass distribution for π^0 candidate is slightly wider in the experiment than in MC. This difference is taken into account by the π^0 efficiency correction, discussed in more detail later.

3.3 Background

The background for the studied decay mode can originate from true e^+e^- interactions or from cosmic particles and beam interactions with the residual gas. The contribution coming from cosmic particles and beam interactions N_{sb} was evaluated considering events from the side-band region $10 < |Z_{trk+}| < 20$ cm, and found to be negligible (less than 0.1%).

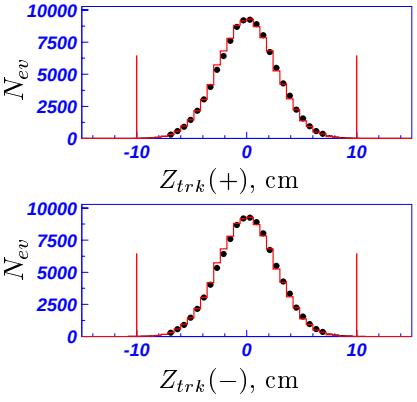

Figure 3: Distribution of the distance from a track to the interaction point along the beam direction Z_{trk}, points correspond to the experimental data, histograms are MC, lines show selection cuts

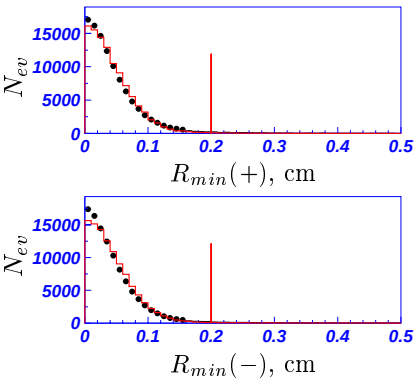

Figure 4: Distribution of the distance from each track to the beam axis in the $(R-\varphi)$ projection R_{min}, points correspond to the experimental data, histograms are MC, lines show selection cuts

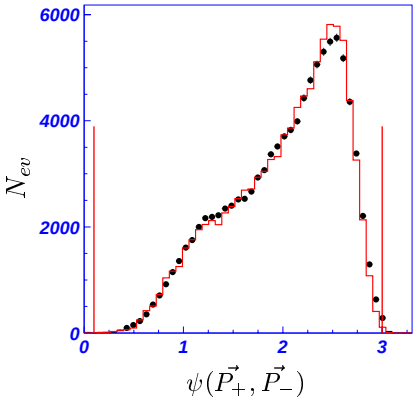

Figure 5: Distribution of the space angle between tracks, points correspond to the experimental data, histogram is MC, lines show selection cuts

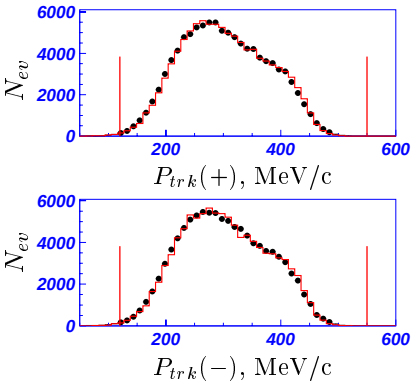

Figure 6: Distribution of the absolute value of track momentum P_{trk}, points correspond to the experimental data, histograms are MC, lines show selection cuts

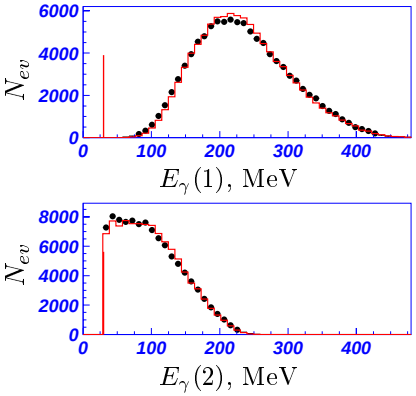

Figure 7: Distributions of the π^0-candidate photon energies, points correspond to the experimental data, histograms are MC, lines show selection cuts

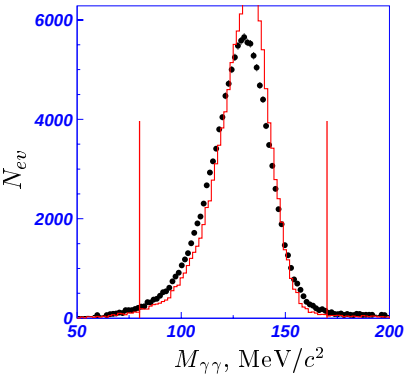

Figure 8: Distribution of the $\gamma\gamma$ invariant mass of π^0-candidate, points correspond to the experimental data, histogram is MC, lines show selection cuts

The main e^+e^- processes which can imitate $e^+e^- \to \pi^+\pi^-\pi^0$ events are:

- $e^+e^- \to \phi \to K_L K_S$ or K^+K^-
- $e^+e^- \to \phi \to \eta\gamma,\ \eta \to \pi^+\pi^-\pi^0$ or $\pi^+\pi^-\gamma$
- $e^+e^- \to \pi^+\pi^-\pi^0\pi^0$
- $e^+e^- \to e^+e^-\gamma(\gamma)$
- $e^+e^- \to \pi^+\pi^-\gamma(\gamma)$
- $e^+e^- \to \mu^+\mu^-\gamma$

To evaluate the number of background events coming from e^+e^- processes we studied the $\gamma\gamma$ invariant mass distribution of π^0 candidates. The signal events group around the π^0 mass, while the $\gamma\gamma$ distribution of background events is flat for all background processes excluding $e^+e^- \to \pi^+\pi^-\pi^0\pi^0$ and $e^+e^- \to \phi \to \eta\gamma,\ \eta \to \pi^+\pi^-\pi^0$ processes (the contribution of the last one is found to be negligible). So, the procedure of background subtraction is the following:

1) First the sample near the ϕ-meson peak (E_{beam} = 509.8 MeV) was analyzed. Here the contribution of each i background e^+e^- process was calculated according to the integrated luminosity L, experimental cross section σ_i and MC detection efficiency ε_i^{MC}. The total number of background events is given by the equation:

$$N_{bg} = N_{sb} + L\sum_i \sigma_i \varepsilon_i^{MC} \tag{2}$$

We found that at the ϕ-meson peak the total background admixture is about 1% mostly from 4π, $\pi\pi\gamma$ and K_LK_S decays.

2) For the 3π sample near the ϕ-meson peak the $\gamma\gamma$ invariant mass distribution was approximated with a sum of logarithmic gaussian $LG(m_{\gamma\gamma})$(see Appendix B) and constant $UNI(m_{\gamma\gamma})$ term:

$$\frac{dN}{dm_{\gamma\gamma}} = N_1 \cdot LG(m_{\gamma\gamma}) + N_2 \cdot UNI(m_{\gamma\gamma}), \tag{3}$$

$$N_1 = n_1^{3\pi} + n_1^{bg},\ N_2 = n_2^{3\pi} + n_2^{bg}, \tag{4}$$

$$UNI(m) = \frac{1}{m_{\max} - m_{\min}},\ m_{min} = 80\ MeV/c^2,\ m_{\max} = 170\ MeV/c^2, \tag{5}$$

where N_1 contains mostly 3π events $n_1^{3\pi}$ with a very small contamination n_1^{bg}, coming from events of the $e^+e^- \to \pi^+\pi^-\pi^0\pi^0$ process, calculated relying on luminosity, cross section and detection efficiency taken from 4π MC simulation – its admixture is found to be less than 0.3%.

The signal events also contribute to the flat part $n_2^{3\pi}$ due to the wrong photon reconstruction. The other source is noise low energy photon taking instead of the real one, which has disappeared in unsensitive part of the detector. Then the number of 3π events is determined $n_2^{3\pi} = N_2 - n_2^{bg}$, where n_2^{bg} was calculated according to Eq.2.

We fix the ratio:

$$\alpha = n_2^{3\pi}/n_1^{3\pi} \tag{6}$$

to use it in our background subtraction procedure for the other energy points (we found it to be 6.9%).

3) To extract the number of signal events at the other energy points the $\gamma\gamma$ invariant mass distribution was approximated by form 3, where the mean value, width, asymmetry of logarithmic gaussian were fixed at their values found from the $\gamma\gamma$ invariant mass spectrum approximation at the ϕ-meson

peak. Free parameters for the i-th energy point are N_1^i and N_2^i. The numbers of signal and background events were calculated according to formulae:

$$N_{3\pi}^i = (1+\alpha)(N_1^i - n_1^{bg}(i)), \tag{7}$$

$$N_{bg}^i = N_2^i - \alpha(N_1^i - n_1^{bg}(i)) + n_1^{bg}(i), \tag{8}$$

where $n_1^{bg}(i)$ is the calculated 4π contribution for the i-th energy point, having a peak in the $m_{\gamma\gamma}$ distribution. The numbers of signal and background events are shown in Table 1. In Fig.9 π^0 candidate $\gamma\gamma$ invariant mass distributions for several energy points are shown with optimal curves, good fit quality for all distributions can be seen.

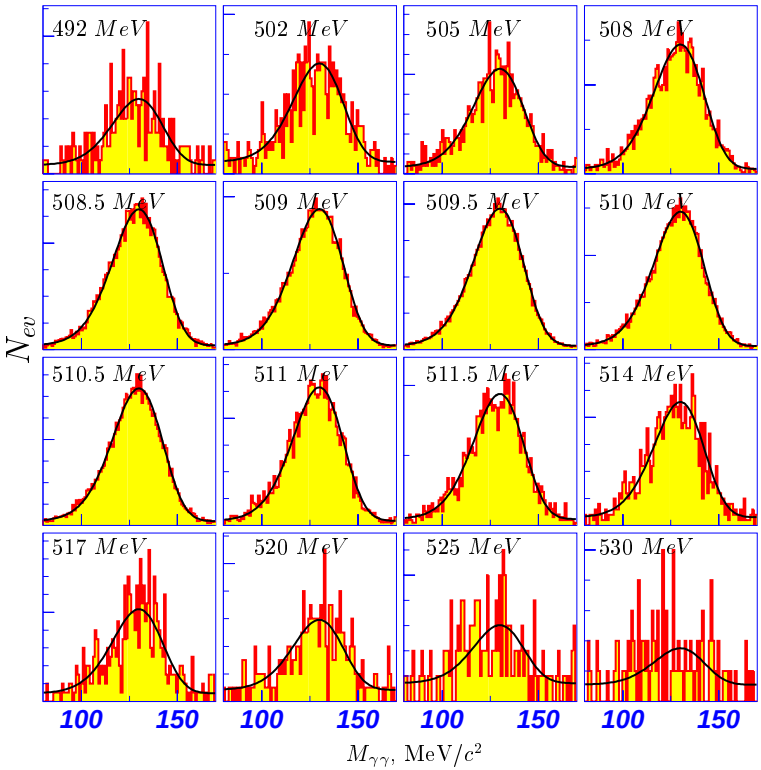

Figure 9: Experimental $M_{\gamma\gamma}$ distributions for 16 energy points. Beam energy is shown for each distribution.

4 Detection efficiency corrections

Monte Carlo simulation can not reproduce all details of the detector response. In this work the corrections to the efficiency $\varepsilon_{3\pi}^{MC}$, obtained by MC, were determined using the experimnetal data.

4.1 Correction to the $\pi^{\pm}$ detection efficiency

To determine the corrections to the $\pi^{\pm}$ detection efficiency from the experimental data two additional sets of signal events were used: with one track and one π^0 (**1TRK**), with two tracks (here more strict cuts to one of the tracks are applied) and one π^0 (**2TRK**).

The number of two-track events:

$$N_{3\pi} = N_0 \varepsilon(\pi^{\pm}\pi^0)\varepsilon(\pi^{\mp}|\pi^{\pm}\pi^0), \tag{9}$$

where

- N_0 – the initial number of $e^+e^- \to \pi^+\pi^-\pi^0$ events,
- $\varepsilon(\pi^{\pm}\pi^0)$ – detection efficiency of the $\pi^{\pm}\pi^0$ subsystem,
- $\varepsilon(\pi^{\mp}|\pi^{\pm}\pi^0)$ – detection efficiency of $\pi^{\mp}$ at a condition that the associated $\pi^{\pm}\pi^0$ subsystem already has been detected. This efficiency can be written as $\varepsilon(\pi^{\mp}|\pi^{\pm}\pi^0) = \varepsilon_{acc}\varepsilon_{rec}\varepsilon_{sel}$, where:
  - ε_{acc} – probability for the pion to hit the sensitive part of the detector;
  - ε_{rec} – reconstruction efficiency;
  - ε_{sel} – efficiency of the selection criteria.

The number of one track events (in the case when the direction of missing track to hit sensitive part of the detector is required):

$$N_{\pi^0\pi^{\pm}} = N_0 \varepsilon(\pi^{\pm}\pi^0)\varepsilon_{acc}(1 - \varepsilon_{rec}\varepsilon_{sel}). \tag{10}$$

The part of the track efficiency related to the reconstruction and selection cuts $\epsilon_{\mp} = \varepsilon_{rec}(\mp)\varepsilon_{sel}(\mp)$ can be determined both from Monte Carlo simulation and experimental data. As a result, an associated correction can be introduced:

$$\frac{N_{2\pi}(\pm)}{N_{3\pi}} = \frac{1}{\epsilon_{\mp}} - 1\,, \tag{11}$$

$$\epsilon_{\mp} = 1/(1 + \frac{N_{2\pi}(\pm)}{N_{3\pi}}), \tag{12}$$

$$\delta_{\mp}^{MC} = 1 - \frac{\epsilon_{\mp}^{EXP}}{\epsilon_{\mp}^{MC}}. \tag{13}$$

As seen from Eq.9, Eq.10 and Eq.12, $\varepsilon(\pi^{\pm}\pi^0)$ cancels in the calculation of $\epsilon_{\mp}$, that is why more strict selection criteria can be applied to a complementary track both in (**1TRK**) and (**2TRK**) events. This allows one to suppress more essentially background in (**1TRK**) events.

To (**1TRK**) sample we select one-track events with the following selection criteria:

- The closest approach of the track to the interaction point in the $R-\varphi$ plane $R_{min} \leq 0.2$ cm and its Z-coordinate $|Z_{trk}| \leq 5$ cm.
- The polar angle of the track and the missing momentum direction should be within: $|\frac{\pi}{2} - \theta| < 0.67$, $|\frac{\pi}{2} - \theta_{mis}| < 0.67$.
- The opening angle between track and missing momentum should be $0.1 < \psi < 3$ to reject collinear events (Bhabha, $\mu\mu$, $\pi\pi$) and events of γ-conversion at the vacuum pipe.
- To suppress radiation Bhabha events we required the ratio of the particle energy deposition in the calorimeter and its momentum to be $\frac{E_{cluster}}{P}(trk) < 0.6$
- Charged particle energy loss per unit pathlength in the DC should be $dE/dx < 2 \cdot dE/dx(MIP)$ to reject charged kaons and protons.
- Absolute value of the track momentum $160 < P_{trk} < 500$ MeV/c.
- Absolute value of the missing momentum $P_{mis} > 110$ MeV/c.
- We select events from the region above the lower boundary of 3π allowed kinematic area.
- Maximal photon energy should be $E_{\gamma max} < 250$ MeV to reject $\eta\gamma$ events.
- Invariant mass of the detected charged pion and missing pion $M_{\pi,missing} > 550$ MeV/c^2 to suppress 4π events

- The π^0 candidate was reconstructed from two γ-quanta with energy threshold $E_\gamma(1,2) > 30$ MeV. and $\gamma\gamma$ invariant mass window $80 \leq M_{\gamma\gamma} \leq 170$ MeV/c^2. If more than two photons were detected, we selected events, where only one π^0 candidate was found among all $\gamma\gamma$ combinations, $N_{\pi^0} = 1$.

The two-track events sample (**2TRK**) is selected according to criteria mentioned in Section 3 (**2T**π^0), also one of the tracks is subjected to the more rigorous criteria described above.

The corrections at different energy points close to the ϕ-meson mass (where we have enough statistics) are shown in Fig.10.

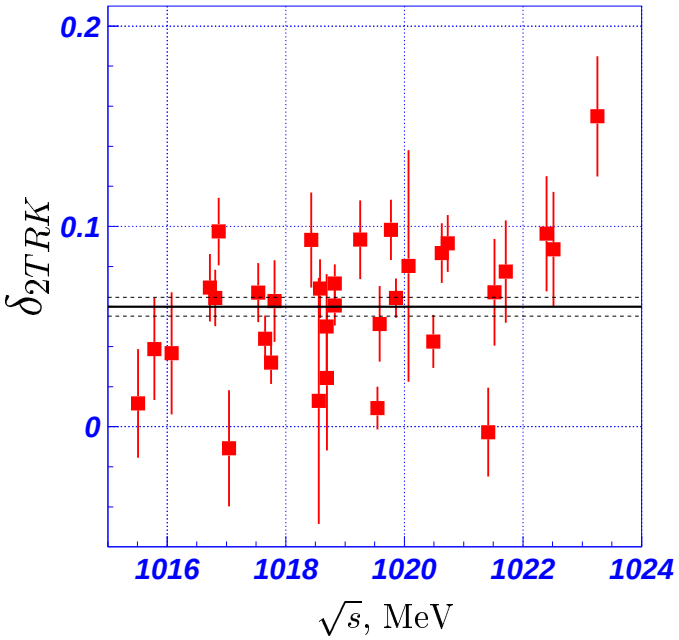

Figure 10: Two-track efficiency correction for different energy points.

For the edge energy points with low statistics we use the average value which is also shown in Fig.10. Applied efficiency corrections are summarized in Table 2.

Table 2: Efficiency corrections. $\delta_+^{MC}(\delta_-^{MC})$ – $\pi^+(\pi^-)$ efficiency correction, $\delta_{2trk}^{MC} = \delta_+^{MC} + \delta_-^{MC} - \delta_+^{MC}\delta_-^{MC}$, $\delta_{\pi^0}^{MC}$ – π^0 efficiency correction, δ^{MC} – the total efficiency correction

#	δ_+^{MC}, %	δ_-^{MC}, %	δ_{2trk}^{MC}, %	$\delta_{\pi^0}^{MC}$, %	δ^{MC}, %
1	2.2 ± 2.6	0.1 ± 2.5	2.4 ± 3.6	7.0 ± 3.8	9.2 ± 5.0
2	-0.1 ± 4.0	1.4 ± 4.6	1.2 ± 6.1	7.3 ± 6.2	8.5 ± 8.3
3	2.4 ± 0.8	3.5 ± 0.9	5.9 ± 1.5	5.5 ± 1.5	11.3 ± 2.3
4	2.4 ± 0.8	3.5 ± 0.9	5.9 ± 1.5	5.5 ± 1.5	11.3 ± 2.3
5	2.4 ± 0.8	3.5 ± 0.9	5.9 ± 1.5	5.5 ± 1.5	11.3 ± 2.3
6	2.9 ± 2.2	0.6 ± 2.1	3.6 ± 3.0	4.0 ± 3.3	7.6 ± 4.3
7	5.4 ± 1.2	4.5 ± 1.2	9.7 ± 1.6	6.1 ± 1.8	15.2 ± 2.2
8	2.3 ± 1.4	4.0 ± 1.5	6.2 ± 2.0	5.6 ± 2.1	11.5 ± 2.8
9	3.1 ± 1.3	6.3 ± 1.5	9.3 ± 1.9	8.5 ± 1.9	17.0 ± 2.5
10	1.7 ± 1.0	5.0 ± 1.1	6.7 ± 1.4	7.3 ± 1.5	13.5 ± 2.0
11	3.4 ± 1.6	6.1 ± 1.8	9.3 ± 2.3	7.5 ± 2.4	16.1 ± 3.1
12	2.5 ± 1.0	4.4 ± 1.1	6.8 ± 1.4	5.2 ± 1.5	11.7 ± 1.9
13	2.0 ± 1.8	3.0 ± 1.9	4.9 ± 2.6	6.0 ± 2.7	10.7 ± 3.6
14	2.1 ± 1.3	3.0 ± 1.4	5.1 ± 1.8	3.9 ± 2.0	8.9 ± 2.6
15	3.9 ± 1.0	6.1 ± 1.1	9.8 ± 1.5	2.1 ± 1.6	11.8 ± 2.0
16	3.6 ± 1.0	5.1 ± 1.1	8.6 ± 1.4	0.0 ± 1.6	8.5 ± 2.1
17	2.3 ± 1.8	4.4 ± 2.0	6.7 ± 2.6	1.4 ± 2.8	8.0 ± 3.7
18	3.6 ± 2.0	6.2 ± 2.2	9.6 ± 2.8	14.4 ± 2.7	22.7 ± 3.4
19	2.4 ± 0.8	3.5 ± 0.9	5.9 ± 1.5	5.5 ± 1.5	11.3 ± 2.3
20	2.4 ± 0.8	3.5 ± 0.9	5.9 ± 1.5	5.5 ± 1.5	11.3 ± 2.3
21	2.4 ± 0.8	3.5 ± 0.9	5.9 ± 1.5	5.5 ± 1.5	11.3 ± 2.3
22	2.4 ± 0.8	3.5 ± 0.9	5.9 ± 1.5	5.5 ± 1.5	11.3 ± 2.3
23	2.4 ± 0.8	3.5 ± 0.9	5.9 ± 1.5	5.5 ± 1.5	11.3 ± 2.3
24	1.4 ± 1.7	2.4 ± 1.8	3.8 ± 2.5	5.6 ± 2.7	9.3 ± 3.6
25	3.7 ± 1.2	3.2 ± 1.2	6.9 ± 1.6	10.0 ± 1.7	16.2 ± 2.1
26	1.9 ± 0.8	2.5 ± 0.8	4.3 ± 1.1	7.8 ± 1.2	11.9 ± 1.5
27	3.2 ± 0.6	4.0 ± 0.7	7.1 ± 0.9	5.4 ± 1.0	12.1 ± 1.3
28	3.1 ± 0.7	3.3 ± 0.7	6.4 ± 0.9	4.9 ± 1.0	11.0 ± 1.3
29	4.5 ± 1.0	4.8 ± 1.0	9.1 ± 1.4	4.1 ± 1.5	12.9 ± 1.9
30	2.1 ± 1.7	5.7 ± 1.9	7.7 ± 2.5	2.9 ± 2.8	10.4 ± 3.5
31	8.0 ± 2.2	8.0 ± 2.3	15.4 ± 3.0	14.0 ± 2.8	27.3 ± 3.5
32	2.4 ± 0.8	3.5 ± 0.9	5.9 ± 1.5	5.5 ± 1.5	11.3 ± 2.3
33	2.4 ± 0.8	3.5 ± 0.9	5.9 ± 1.5	5.5 ± 1.5	11.3 ± 2.3
34	2.4 ± 0.8	3.5 ± 0.9	5.9 ± 1.5	5.5 ± 1.5	11.3 ± 2.3
35	2.4 ± 0.8	3.5 ± 0.9	5.9 ± 1.5	5.5 ± 1.5	11.3 ± 2.3

36	2.4 ± 0.8	3.5 ± 0.9	5.9 ± 1.5	5.5 ± 1.5	11.3 ± 2.3
37	2.4 ± 0.8	3.5 ± 0.9	5.9 ± 1.5	5.5 ± 1.5	11.3 ± 2.3
38	2.4 ± 0.8	3.5 ± 0.9	5.9 ± 1.5	5.5 ± 1.5	11.3 ± 2.3
39	2.4 ± 0.8	3.5 ± 0.9	5.9 ± 1.5	5.5 ± 1.5	11.3 ± 2.3
40	-1.7 ± 1.7	2.8 ± 2.0	1.1 ± 2.7	7.1 ± 2.8	8.2 ± 3.7
41	3.9 ± 1.0	2.6 ± 1.0	6.4 ± 1.4	8.2 ± 1.4	14.1 ± 1.8
42	0.8 ± 0.7	2.3 ± 0.7	3.1 ± 1.0	6.3 ± 1.1	9.3 ± 1.4
43	2.6 ± 0.7	3.4 ± 0.7	6.0 ± 1.0	6.7 ± 1.0	12.4 ± 1.3
44	-0.3 ± 0.7	1.3 ± 0.7	0.9 ± 1.0	4.5 ± 1.1	5.4 ± 1.5
45	0.7 ± 0.9	3.5 ± 0.9	4.2 ± 1.3	0.4 ± 1.4	4.7 ± 1.9
46	0.4 ± 1.5	-0.7 ± 1.5	-0.2 ± 2.2	2.0 ± 2.4	1.8 ± 3.2
47	2.2 ± 2.0	6.7 ± 2.2	8.8 ± 2.8	1.1 ± 3.0	9.8 ± 4.0
48	2.4 ± 0.8	3.5 ± 0.9	5.9 ± 1.5	5.5 ± 1.5	11.3 ± 2.3
49	2.4 ± 0.8	3.5 ± 0.9	5.9 ± 1.5	5.5 ± 1.5	11.3 ± 2.3
50	2.4 ± 0.8	3.5 ± 0.9	5.9 ± 1.5	5.5 ± 1.5	11.3 ± 2.3
51	2.4 ± 0.8	3.5 ± 0.9	5.9 ± 1.5	5.5 ± 1.5	11.3 ± 2.3
52	2.4 ± 0.8	3.5 ± 0.9	5.9 ± 1.5	5.5 ± 1.5	11.3 ± 2.3
53	-0.7 ± 1.9	-0.3 ± 2.0	-1.0 ± 2.8	-3.0 ± 3.4	-4.1 ± 4.5
54	4.8 ± 4.2	3.3 ± 4.2	8.0 ± 5.7	4.2 ± 6.2	11.9 ± 7.9

4.2 Correction to the π^0 detection efficiency

To determine the corrections to the π^0 detection efficiency from the experimental data two sets of signal events were used: ($\mathbf{2T}\pi^0$) and with two tracks ($\mathbf{2T}$) (without any criteria concerning π^0) .

The number of ($\mathbf{2T}\pi^0$) events:

$$N_{3\pi} = N_0 \varepsilon(\pi^+\pi^-)\varepsilon(\pi^0|\pi^+\pi^-), \tag{14}$$

where:

- N_0 – initial number of 3π events;
- $\varepsilon(\pi^+\pi^-)$ – detection efficiency of $\pi^+\pi^-$ subsystem;
- $\varepsilon(\pi^0|\pi^+\pi^-)$ – detection efficiency of π^0 in condition when associated $\pi^+\pi^-$ subsystem has been already detected.

The number of two track events ($\mathbf{2T}$):

$$N_{\pi^+\pi^-} = N_0 \varepsilon(\pi^+\pi^-). \tag{15}$$

As a result:

$$\epsilon_{\pi^0} = \varepsilon(\pi^0|\pi^+\pi^-) = N_{3\pi}/N_{\pi^+\pi^-} \tag{16}$$

ϵ_{π^0} can be calculated both from Monte Carlo simulation and experimental data, so the correction to the π^0 detection efficiency:

$$\delta^{MC}_{\pi^0} = 1 - \epsilon^{EXP}_{\pi^0}/\epsilon^{MC}_{\pi^0}. \tag{17}$$

The π^0 corrections at different energy points are shown in Fig.11.

Applied π^0 efficiency corrections are also summarized in the Table 2.

Finally, total detection efficiency correction δ^{MC} is determined by formula:

$$(1 - \delta^{MC}) = (1 - \delta^{MC}_{-})(1 - \delta^{MC}_{+})(1 - \delta^{MC}_{\pi^0}). \tag{18}$$

The δ^{MC} for different energy points is shown in Table 2. For edge energy points we use the value averaged over corrections at different energy points near ϕ-meson mass. Figure 12 demonstrates the distribution of the total efficiency correction.

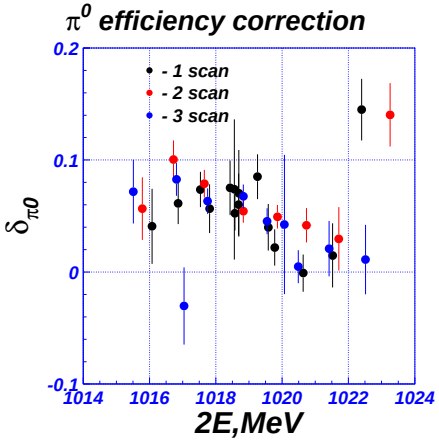

Figure 11: π^0 efficiency correction for different energy points.

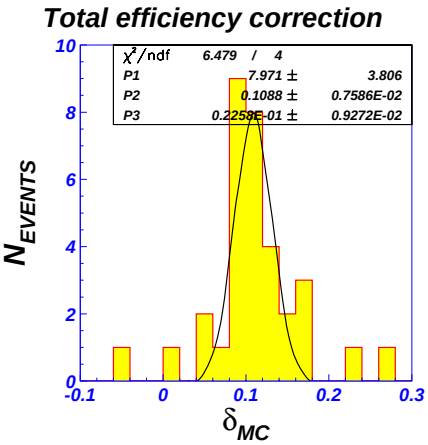

Figure 12: Distribution of the total efficiency correction δ^{MC}

5 Cross section determination

5.1 Visible cross section

The number of detected 3π events corresponding to the integrated luminosity of $\mathcal{L} = \int Ldt$, is given by the formula:

$$N_{3\pi} = \mathcal{L}\varepsilon\sigma_{exp}\,, \tag{19}$$

where ε is 3π detection efficiency, σ_{exp} is an experimental cross section of $e^+e^- \to \pi^+\pi^-\pi^0$.

In our analysis the total detection efficiency consists of several parts:

$$\varepsilon = \varepsilon_{trig}\varepsilon_{3\pi}^{MC}(1-\delta^{MC}), \tag{20}$$

where ε_{trig} is a trigger efficiency, $\varepsilon_{3\pi}^{MC}$ is 3π MC detection efficiency (see the Section 3), δ^{MC} is the correction to the $\varepsilon_{3\pi}^{MC}$ from the experimental data (see the Section 4).

The experimental cross section σ_{exp} is given by the equation:

$$\sigma_{exp} = (1+\delta_{wid})(1+\delta_{rad})\sigma_B, \tag{21}$$

where the effect of the beam energy spread is taken into account by δ_{wid}, which is discussed in more detail in Appendix **A**. δ_{rad} is a correction due to the initial state radiation, which will be discussed later. σ_B is Born cross section of $e^+e^- \to \pi^+\pi^-\pi^0$ reaction. As a result, the 3π Born cross ection is calculated according to the formula:

$$\sigma_B = \frac{N_{3\pi}}{\mathcal{L}\varepsilon_{trig}\varepsilon_{3\pi}^{MC}(1+\delta_{rad})(1+\delta_{wid})(1-\delta^{MC})}. \tag{22}$$

The visible cross section σ_{vis} is introduced as Born 3π cross section with effects of ISR:

$$\sigma_{vis} = (1+\delta_{rad})\sigma_B = \frac{N_{3\pi}}{\mathcal{L}\varepsilon_{trig}\varepsilon_{3\pi}^{MC}(1+\delta_{wid})(1-\delta^{MC})}. \tag{23}$$

All related numbers can be found in Tables 1,2 and 3.

Table 3: The cross section data. MC detection efficiency $\varepsilon_{3\pi}^{MC} = 4.71 \pm 0.02\%$. $\mathcal{L}$ – luminosity; ε_{trig} – trigger efficiency, its error is about 0.1% for all energy points; δ_{wid} - correction due to the beam enery spread, its error is less than 0.1% for all energy points; δ_{rad} – radiation correction; σ_{vis} – visible cross section; σ_B – Born cross section.

#	$\mathcal{L}$, nb^{-1}	ε_{trig}, %	δ_{wid}	δ_{rad}	σ_{vis}, nb	σ_B, nb
1	29.91±0.31	99.1	−3.8	−0.2678±0.0011	449.35±34.91	613.72±47.78
2	9.25±0.17	99.1	−3.4	−0.2708±0.0010	447.47±60.03	613.67±82.61
3	110.54±0.55	99.6	0.0	−0.1312±0.0010	16.52± 2.55	19.01± 2.94
4	115.50±0.62	98.8	0.1	−0.1824±0.0009	21.73± 3.29	26.58± 4.26
5	165.12±0.78	98.9	0.4	−0.2191±0.0007	47.77± 3.73	61.17± 4.92
6	111.62±0.68	98.0	1.8	−0.2681±0.0004	171.75±11.05	234.66±15.27
7	237.80±0.95	98.2	1.6	−0.2750±0.0004	264.92± 9.70	365.45±13.70
8	111.13±1.00	98.3	−0.5	−0.2784±0.0007	356.99±16.04	494.74±22.56
9	126.76±0.71	99.1	−3.7	−0.2484±0.0012	459.51±18.88	611.44±25.23
10	253.78±0.95	98.3	0.4	−0.2784±0.0006	334.98±10.57	464.25±14.86
11	75.27±0.51	99.1	−3.0	−0.2730±0.0009	452.68±22.81	622.74±31.47
12	234.92±0.91	99.1	−3.5	−0.2704±0.0010	447.12±13.42	612.83±18.43
13	67.83±0.49	99.1	−3.8	−0.2678±0.0010	433.91±23.73	592.69±32.47
14	117.34±0.66	99.1	−2.5	−0.2317±0.0014	460.68±18.25	599.69±23.83
15	227.89±0.98	99.8	−1.5	−0.2201±0.0014	434.95±13.39	557.75±17.36
16	224.74±0.92	99.7	1.9	−0.1546±0.0021	322.96±10.44	382.04±12.58
17	117.25±0.66	99.8	3.0	−0.0676±0.0035	216.75±11.81	232.47±12.83
18	163.78±0.79	99.8	2.8	0.0323±0.0055	163.97± 9.72	158.84± 9.50
19	180.87±0.82	99.8	1.1	0.9649±0.0525	37.30± 3.06	18.98± 1.65
20	152.85±0.75	99.3	0.7	3.687± 0.566	17.15± 2.07	3.66± 0.62
21	126.89±0.73	99.5	0.7	13.82± 2.59	11.20± 1.87	0.81± 0.20
22	179.81±0.87	99.6	0.0	16.12± 16.12	3.52± 1.55	0.20± 0.20
23	157.41±0.75	98.9	0.4	−0.2179±0.0006	52.12± 3.75	66.65± 4.93
24	142.25±0.71	98.0	1.7	−0.2652±0.0004	169.64± 9.38	230.87±12.91
25	269.42±0.98	98.2	1.7	−0.2739±0.0004	246.59± 8.80	339.65±12.26
26	433.23±1.25	98.3	0.1	−0.2785±0.0006	336.58± 8.23	466.54±11.50
27	579.24±1.47	99.1	−4.0	−0.2642±0.0011	460.78± 9.04	626.24±12.33
28	582.46±1.53	99.8	−1.1	−0.2149±0.0014	414.82± 8.30	528.37±10.64
29	351.00±1.20	99.7	2.2	−0.1458±0.0023	304.01± 8.91	355.90±24.00
30	156.80±0.82	99.8	3.0	−0.0470±0.0037	181.77± 9.69	190.74±13.57
31	227.48±1.01	99.3	2.4	0.1448±0.0083	119.89± 7.58	104.72± 6.69
32	178.05±0.85	99.8	1.0	1.1485±0.0620	32.23± 2.90	15.00± 1.42

33	163.09±0.82	99.3	0.7	4.0683±0.6341	16.53± 2.02	3.26± 0.57
34	178.59±0.82	99.5	0.7	13.34± 2.81	12.64± 1.84	0.88± 0.21
35	210.27±0.90	98.7	3.0	54.76± 54.76	5.62± 1.43	0.10± 0.10
36	168.29±0.76	98.8	0.1	−0.1824±0.0009	29.35± 2.88	35.90± 3.79
37	194.78±0.79	99.6	0.0	−0.1311±0.0010	14.27± 1.93	16.43± 2.22
38	158.57±0.70	98.8	0.1	−0.1824±0.0009	28.32± 2.94	34.64± 3.86
39	163.42±0.72	98.9	0.4	−0.2152±0.0007	47.02± 3.73	59.92± 7.20
40	144.69±0.67	98.0	1.6	−0.2624±0.0004	151.72± 8.77	205.71±14.65
41	402.70±1.15	98.2	1.6	−0.2746±0.0005	259.70± 7.60	358.05±17.39
42	462.62±1.23	98.3	−0.3	−0.2785±0.0007	358.41± 8.08	496.77±11.31
43	415.08±1.23	99.1	−4.0	−0.2641±0.0011	468.55±10.03	636.74±13.67
44	401.18±1.14	99.1	−2.6	−0.2338±0.0014	458.07± 9.93	597.86±13.08
45	318.17±1.05	99.7	1.5	−0.1671±0.0019	329.95± 9.03	396.19±10.98
46	174.65±0.76	99.8	3.0	−0.0788±0.0033	195.80± 8.98	212.55± 9.89
47	156.43±0.72	99.3	2.8	0.0466±0.0058	124.46± 7.81	118.91± 7.70
48	210.87±0.87	99.8	1.1	0.9675±0.0501	36.71± 2.72	18.65± 1.47
49	203.74±0.84	99.3	0.7	3.6413±0.5563	17.76± 2.12	3.82± 0.64
50	147.07±0.75	99.5	0.7	12.43± 2.59	7.10± 1.88	0.52± 0.17
51	106.68±0.63	98.7	4.6	56.94± 56.94	8.34± 2.01	0.14± 0.14
52	59.73±0.48	99.6	0.0	17.35± 17.35	8.97± 2.37	0.48± 0.47
53	73.70±0.48	98.2	1.4	−0.2762±0.0005	255.06±15.33	352.44±24.37
54	15.07±0.22	99.8	−0.1	−0.2000±0.0016	409.74±48.82	512.23±62.52

5.2 Trigger efficiency

CMD-2 had two independent trigger subsystems:

- **Neutral trigger system**(NT) which produces the trigger signal based on the information from the calorimeter, its efficiency for 3π events is ε_{NT};
- tracking subsystem (ZC and DC) based **charged trigger**(QT) uses the information about DC,ZC hits, its efficiency for 3π events is ε_{QT};

3π events were recorded when NT **or** QT signal appeared. As a result, the total trigger efficiency for 3π events is:

$$\varepsilon_{trig} = 1 - (1 - \varepsilon_{NT})(1 - \varepsilon_{QT}). \tag{24}$$

We determine ε_{NT} and ε_{QT} from the experimental data. Counting events with neutral trigger $N(NT)$, charged trigger $N(QT)$ and with both triggers $N(NT\&QT)$ we calculate efficiencies according to equations:

$$\varepsilon_{NT} = \frac{N(NT\&QT)}{N(QT)}, \tag{25}$$

$$\varepsilon_{QT} = \frac{N(QT\&NT)}{N(NT)}. \tag{26}$$

Figure 13 shows the trigger efficiency value at different energy points (see also the Table 3). It can be seen that ε_{trig} is high (more than 98%) for all energy points.

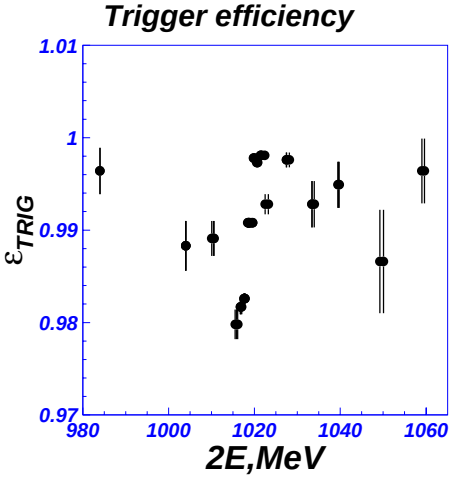

Figure 13: Trigger efficiency ε_{trig} for different c.m. energy points.

6 Cross section approximation

The important issue for the evaluation of σ_B is a correct account of the radiation correction, i.e. contribution of ISR and high order diagrams. In this work the approach developed in [16] was used. This model assumes that both electron and positron emit photon jets in the forward direction. In this case the visible cross section is related to σ_B as:

$$\sigma_{vis}(s) = \int_0^1 dx_1 \int_0^1 dx_2 D(x_1,s)D(x_2,s)\sigma_B(s(1-x_1)(1-x_2))\varepsilon(x_1,x_2) =$$

$$= (1+\delta_{rad}(s))\sigma_B(s), \tag{27}$$

where $\delta_{rad}(s)$ is a radiation correction, presented in Table 3.

In Eq.27:

- $D(x_{1,2}, s)$ – probability function for initial $e^{\pm}$ to emit γ-quant jet carrying $x_{1,2} = \frac{2E_{\gamma 1,2}}{\sqrt{s}}$ part of $e^{\pm}$ energy $\sqrt{s}/2$;
- $\sigma_B(s(1-x_1)(1-x_2))$ – 3π Born cross section at the new c.m. energy;
- $\varepsilon(x_1, x_2)$ – efficiency function, which is defined as a detection efficiency for boosted (due to γ-quanta radiation) $\pi^+\pi^-\pi^0$ system, normalized to that at $x_1 = x_2 = 0$.

Figure 14 shows $\varepsilon(x_1, x_2)$, that calculated using 3π MC simulation of 10^6 events with initial state radiation.

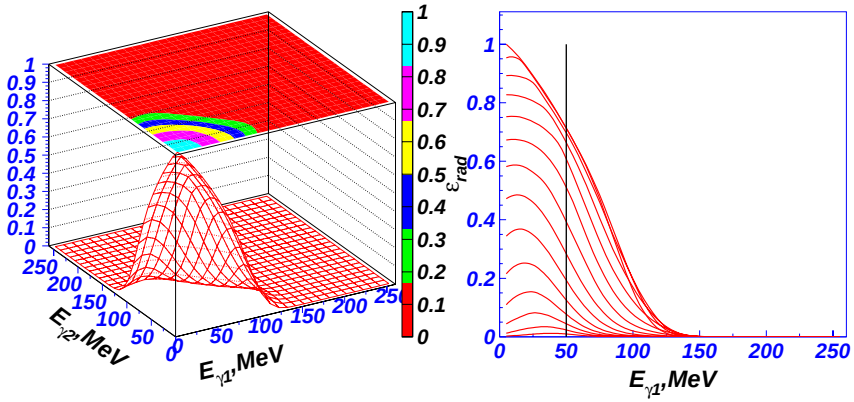

Figure 14: Efficiency function depending on the ISR γ-quants energies(left); efficiency dependence on the energy of the first γ-quant for a fixed values of the second γ-quant energy.

6.1 Born $e^+e^- \to \pi^+\pi^-\pi^0$ cross section

The Born cross section was described by the ω and ϕ contributions:

$$\sigma_{3\pi}(s) = \frac{F_{3\pi}(s)}{s} \cdot |A_\omega + A_\phi e^{i\delta_{\phi-\omega}} + A_{add}|^2, \tag{28}$$

$$A_V = \frac{m_V^2 \Gamma_V \sqrt{\sigma_V / F_{3\pi}(m_V^2)}}{s - m_V^2 + i\sqrt{s}\Gamma_V(s)}, \; V = \omega, \phi\,, \tag{29}$$

where m_V, Γ_V, σ_V – mass, width and peak cross section of the intermediate ω or ϕ vector meson, $\delta_{\phi-\omega}$ – relative phase of $\phi-\omega$ interference, $F_{3\pi}(s)$ – smooth function, which is written as integral over the kinematically allowed region on the E_+ $VS.$ E_- plane:

$$F_{3\pi}(s) = \int\int dE_- dE_+ |\vec{p}_+ \times \vec{p}_-|^2 R_{3\pi}(E_+, E_-), \tag{30}$$

where $E_+, E_-, \vec{p}_+, \vec{p}_-$ – energies and momenta of charged pions, $|\vec{p}_+ \times \vec{p}_-|^2$ – factor reflecting the properties of vector particle decay into three pseudoscalars and $R_{3\pi}(E_+, E_-)$ – function characterizing $\phi \to \pi^+\pi^-\pi^0$ decay dynamics. Assuming that the 3π final state is a combination of $\rho\pi$ amplitude with a constant one ($A_n = 7.52, a = 0.103 \pm 0.028$, $\varphi = -2.0 \pm 0.3$ [13]) $R_{3\pi}(E_+, E_-)$ can be written as:

$$R_{3\pi}(E_+, E_-) = 1/D_{\rho^+}(Q_+^2) + 1/D_{\rho^-}(Q_-^2) + 1/D_{\rho^0}(Q_0^2) + A_n a e^{i\varphi}, \tag{31}$$

where $1/D_{\rho^i}(Q_i^2)$ – ρ^i-meson ($i = +, -, 0$) propagator with its squared four-momentum Q_i^2.

$$1/D_{\rho^i} = \frac{1}{\frac{Q_i^2}{M_\rho^2} - 1 + i\frac{\sqrt{Q_i^2}\Gamma_\rho(Q_i^2)}{M_\rho^2}}. \tag{32}$$

The A_{add} term in Eq.28 takes into account the contributions of the higher mass vector resonances, such as ω' and ω'' around the ϕ-meson.

The energy-dependent widths for both ω and ϕ are written as a sum of their main decay modes partial widths:

$$\Gamma_\phi(s) = \Gamma_\phi \cdot \Big(B_{K^+K^-}\frac{m_\phi^2 F_{K^+K^-}(s)}{sF_{K^+K^-}(m_\phi^2)} + B_{K_SK_L}\frac{m_\phi^2 F_{K_SK_L}(s)}{sF_{K_SK_L}(m_\phi^2)} + $$

$$+ B_{\eta\gamma}\frac{F_{\eta\gamma}(s)}{F_{\eta\gamma}(m_\phi^2)} + B_{3\pi}\frac{\sqrt{s}F_{3\pi}(s)}{m_\phi F_{3\pi}(m_\phi^2)}\Big), \tag{33}$$

$$\Gamma_\omega(s) = \Gamma_\omega \cdot \Big(B_{\pi^+\pi^-}\frac{m_\omega^2 F_{2\pi}(s)}{sF_{2\pi}(m_\omega^2)} + B_{\pi^0\gamma}\frac{F_{\pi^0\gamma}(s)}{F_{\pi^0\gamma}(m_\omega^2)} + B_{3\pi}\frac{\sqrt{s}F_{3\pi}(s)}{m_\omega F_{3\pi}(m_\omega^2)}\Big), \tag{34}$$

where:

$$F_{\pi\pi}(s) = (s/4 - m_\pi^2)^{3/2},\ F_{K\bar{K}}(s) = (s/4 - m_K^2)^{3/2}, \tag{35}$$

$$F_{\pi^0\gamma}(s) = (\sqrt{s}(1 - m_{\pi^0}^2/s))^3,\ F_{\eta\gamma}(s) = (\sqrt{s}(1 - m_\eta^2/s))^3. \tag{36}$$

6.2 Fitting of the $e^+e^- \to \pi^+\pi^-\pi^0$ cross section

The experimental $\sigma_{vis}(s)$ values were approximated by the function given by Eq.27.

Table 4 shows the results of two fits.

Table 4: Result of the visible cross section approximation

Parameters	Fit №1	Fit №2
m_ϕ, MeV/c^2	1019.30 ± 0.02	1019.33 ± 0.03
Γ_ϕ, MeV	4.30 ± 0.06	4.26 ± 0.06
$\varphi^o_{\phi-\omega}$	167 ± 14	$180 - fixed$
$\sigma_{3\pi}$, nb	637 ± 23	658 ± 7
A_{add}, $\sqrt{\text{nb}}$/MeV^2	$0 - fixed$	22 ± 8
χ^2/Ndf	57.0/50	51.8/50
$P(\chi^2), \%$	23	40

For both fits ϕ-meson mass m_ϕ, its width Γ_ϕ and 3π peak cross section $\sigma_{3\pi}$ were free parameters. Our sensitivity is not enough to keep free both $\phi - \omega$ interference phase $\varphi_{\phi-\omega}$ and A_{add} amplitude. So $\varphi_{\phi-\omega}$ is free in the Fit №1 and it is fixed at 180^o value in the Fit №2. All the other parameters were fixed at their world average values [17] within their uncertainties, they are shown in Table 5.

Figure 15 demonstrates visible cross section experimental data with optimal curve for Fit№1.

Table 5: Fixed ω and ϕ-meson parameters

$\omega(782)$	$M = 782.59 \pm 0.11$ MeV/c^2	$\Gamma = 8.49 \pm 0.08$ MeV	$\sigma_{peak} = 1524 \pm 24$ nb
	$Br(3\pi) = 0.891 \pm 0.007$	$Br(\pi\gamma) = 0.0892 \pm 0.0026$	$Br(2\pi) = 0.017 \pm 0.003$
$\phi(1020)$	$Br(K^+K^-) = 0.491 \pm 0.006$	$Br(K_SK_L) = 0.340 \pm 0.005$	
	$Br(3\pi) = 0.155 \pm 0.005$	$Br(\eta\gamma) = 0.01295 \pm 0.00025$	

From Table 4 good fit quality can be seen for both approximations.

To get 3π Born cross section we calculate the radiation correction according to Eq.27 and then apply it the to visible cross section:

$$\sigma_B(s) = \sigma_{vis}(s)/(1 + \delta_{rad}(s))\,. \tag{37}$$

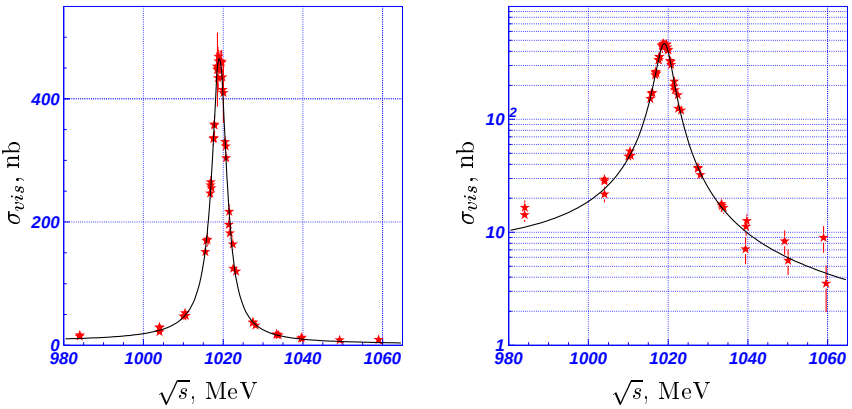

Figure 15: Visible cross section with optimal curve for Fit№1, left – linear scale, right – logarithmic scale

To calculate additional uncertainty related to radiation correction for a particular set of optimal parameters we generated 10^4 such sets. Each parameter was generated according to the Gaussian distribution with mean value equal to its fit optimal value and RMS equal to the fit error (correlation between fit parameters were not taken into account). For each set of parameters we calculate $\delta_{rad}(s)$, so for many sets we have the peaking distribution over δ_{rad}. The RMS of this distribution is taken as uncertainty of the δ_{rad}. It should be noted that the δ_{rad} uncertainty is 100% in the region of born cross section dip at $\sqrt{s} = 1050 \div 1060$ MeV.

Fig.16 demonstrates Born cross section data with optimal Fit№1 curve.

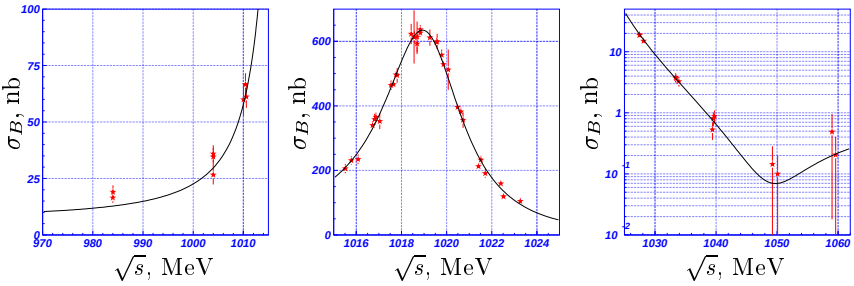

Figure 16: Born cross section with optimal Fit№1 curve for three c.m. energy diapasons

6.3 Systematic uncertainties

The systematic uncertainty in the ϕ-meson mass – m_ϕ is evaluated to be 0.1 MeV, which is related to the energy calculation procedure. The systematic uncertainties in the total ϕ-meson width – Γ_ϕ and $\phi - \omega$ interference phase – $\varphi_{\phi-\omega}$ were evaluated approximating cross section data for three different energy scans, they were found to be 0.17 MeV and 10^o respectively. The main sources of $\sigma_{3\pi}$ systematic uncertainty are shown in Table. 6

Table 6: The main sources of $\sigma_{3\pi}$ systematic uncertainty

Source	Value
Luminosity	2%
Trigger efficiency	1%
Radiation correction	1%
Detection efficiency	0.5%
Background subtraction	0.3%
Total	2.5%

The dominant contribution comes from uncertainty in the integrated luminosity (2%). The systematic uncertainty in radiation correction is determined by the efficiency function $\varepsilon(x_1, x_2)$ error ($\approx$ 1%) and uncertainty of technique itself (0.2%) [16]. The systematic uncertainty in the detection efficiency consists of 0.4% uncertainty due to the limited 3π MC statistics, 0.3% uncertainty in the tracks efficiency correction and 0.2% uncertainty in the π^0 efficiency correction. The 0.3% systematic uncertainty due to the background subtraction was found applying two different background subtraction procedures.

6.4 Result and discussion

Our result on ϕ-meson parameters:

$$m_\phi = (1019.30 \pm 0.02_{stat} \pm 0.10_{syst}) \text{ MeV/c}^2 ,$$

$$\Gamma_\phi = (4.30 \pm 0.06_{stat} \pm 0.17_{syst}) \text{ MeV},$$

$$\varphi_{\phi-\omega} = 167^o \pm 14^o_{stat} \pm 10^o_{syst}$$

and they do not contradict to the world average values [17].

Our result on the 3π peak cross section is:

$$\sigma_{3\pi} = (637 \pm 23_{stat} \pm 16_{syst}) \text{ nb} \ .$$

We calculate the product of the $\phi \to \pi^+\pi^-\pi^0$ branching ratio and $\phi \to e^+e^-$ $Br_{ee}Br_{3\pi}$ according to the relation:

$$B_{ee}B_{3\pi} = \frac{\sigma_{3\pi} M_\phi^2}{12\pi} \, . \tag{38}$$

Our result, the most precise previous results, coming from CMD-2 [6], SND [18] and Babar [19] studies as well as the world average $Br_{ee}Br_{3\pi}$ value [17] are shown in Table 7 and Fig.17.

Table 7: $Br_{ee}Br_{3\pi}$ data

Work	$Br_{ee}Br_{3\pi}$, 10^{-5}
CMD2-1998	$4.35 \pm 0.27 \pm 0.08$
SND-2001	$4.665 \pm 0.042 \pm 0.261$
Babar-2004	$4.30 \pm 0.08 \pm 0.21$
PDG2004-average	4.52 ± 0.19
this work	$4.51 \pm 0.16 \pm 0.11$

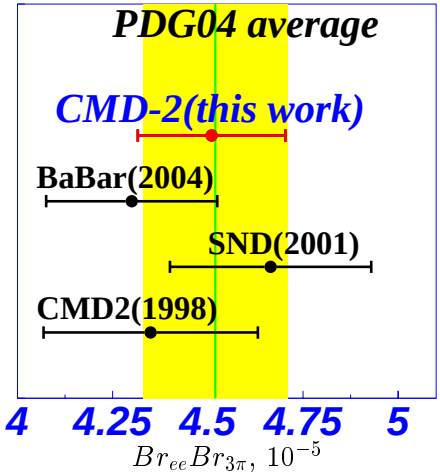

Figure 17: $Br_{ee}Br_{3\pi}$ result for several experiments.

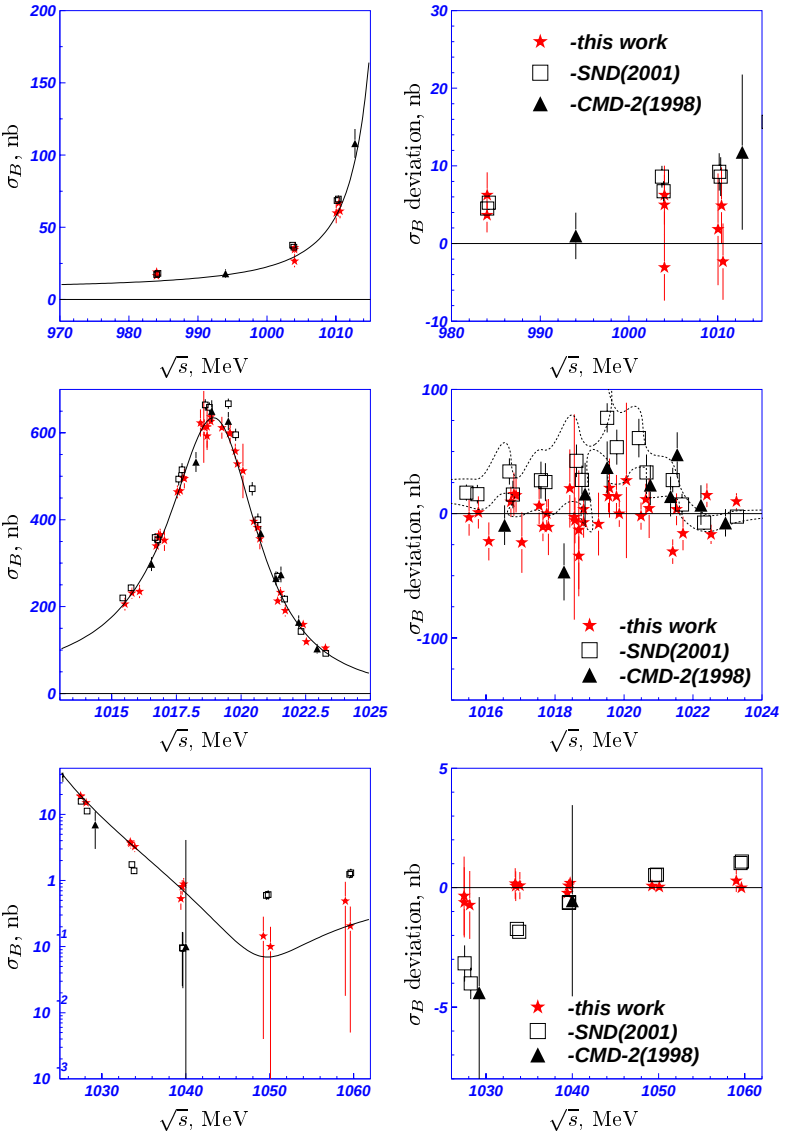

Figure 18: Comparison of 3π Born cross section measured in this work, SND(2001) and CMD-2(1998) for different energy ranges. Left column – the cross sections, right column – the deviation of cross sections from our optimal curve.

Our result is in good agreement with previous measurements and has the best total accuracy.

Figure 18 shows the comparison of the Born cross section obtained in this work and in the previous study of $e^+e^- \to \pi^+\pi^-\pi^0$ with CMD-2 [6] and SND [18] for three energy regions.

Good agreement with the previous CMD-2 study is observed for a whole energy range, while one can note a small deviation of our data from SND points at the right side of the ϕ-meson curve ($\pm 5\%$ SND cross section systematics region is shown between dashed curves in the right middle plot of Fig.18).

7 Analysis of $\phi \to \pi^+\pi^-\pi^0$ dynamics

For this analysis the Dalitz plot shown schematically in Fig.19 was used.

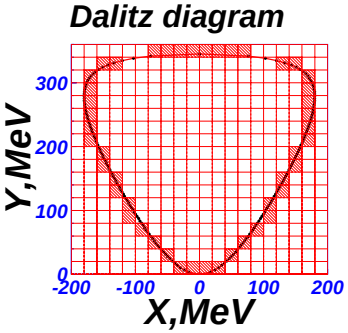

Figure 19: Dalitz diagram; $X = \frac{E_{\pi^-} - E_{\pi^+}}{\sqrt{3}}$, $Y = \sqrt{s} - E_{\pi^-} - E_{\pi^+} - m_{\pi^0}$, solid curve marks the boundary of 3π kinematically allowed region.

The kinematicaly allowed region was divided into 198 square bins of 20×20 MeV size. Hatched bins near the boundary were excluded from analysis. 79577 experimental 3π events from the c.m. energy range $\sqrt{s} = 1017 \div 1021$ MeV were selected for further Dalitz analysis. In addition to the selection criteria mentioned in Section 3 constrained fit, taking into account total energy and momentum conservation law was applied.

For the analysis we take the model incorporating $\rho\pi$ mechanism and non-$\rho\pi$ contribution described by contact amplitude (see Fig.20).

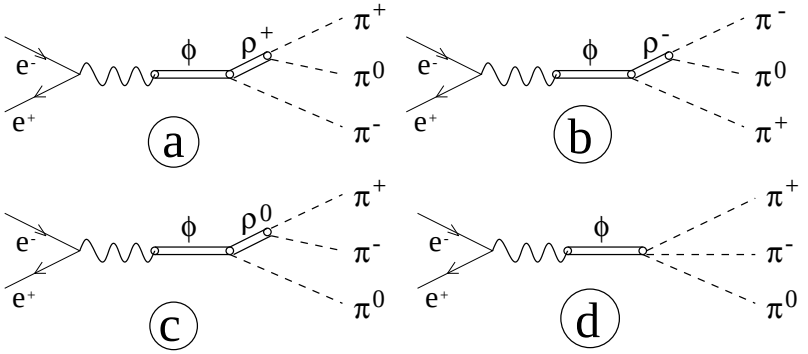

Figure 20: $\phi \to \pi^+\pi^-\pi^0$ decay mechanism. a),b),c) show the $\rho\pi$ contributions; d) shows the contact term.

The theoretical number of events in the bin number k is given by expression:

$$N_k^{th} = \frac{N_0}{Z}\int_k dXdY|\vec{P_+} \times \vec{P_-}|^2|A_n a e^{i\varphi} + A_{\rho\pi}|^2, \tag{39}$$

where Z is normalization constant given by formula:

$$Z = \sum_{k=1}^{198}\int_k dXdY|\vec{P_+} \times \vec{P_-}|^2|A_n a e^{i\varphi} + A_{\rho\pi}|^2, \tag{40}$$

N_0 – total number of 3π events, $A_{\rho\pi}$ – $\rho\pi$ contribution to the amplitude, determined by formula:

$$A_{\rho\pi} = \frac{1}{D_{\rho^+}(Q_+^2)} + \frac{1}{D_{\rho^-}(Q_-^2)} + \frac{1}{D_{\rho^0}(Q_0^2)}, \tag{41}$$

where ρ^i-meson ($i = +, -, 0$) propagator is written in the form:

$$\frac{1}{D_{\rho^i}(Q_i^2)} = \frac{1}{\frac{Q_i^2}{M_\rho^2} - 1 + i\frac{\sqrt{Q_i^2}\Gamma_\rho(Q_i^2)}{M_\rho^2}}. \tag{42}$$

The non-$\rho\pi$ amplitude includes $A_n = 7.52$ – normalization coefficient determined by expression:

$$\int_{Dalitz} dXdY|\vec{P_+} \times \vec{P_-}|^2|A_{\rho\pi}|^2 = |A_n|^2\int_{Dalitz} dXdY|\vec{P_+} \times \vec{P_-}|^2, \tag{43}$$

a – absolute value of normalized contact amplitude, φ - phase of contact amplitude.

The calculated number of events in the i-th cell is given by expression:

$$N_i^{calc} = \varepsilon_{ik} N_k^{theory}, \tag{44}$$

where ε_{ik} is 198×198 matrix of detector apparatus function.

Due to the imperfect reconstruction and a finite resolution of detector 3π event initially produced to the bin number k can be found in the bin number i, so along with detection efficiency for every bin ε_{ik} provides the table of bin-to-bin transition probabilities. ε_{ik} also takes into account the effect of Dalitz plot distortion due to the initial state γ-quanta radiation. We use full MC simulation with ISR to extract ε_{ik}. The graphical example of the table for one bin is shown on Fig.21. The influence of background was found to be negligible.

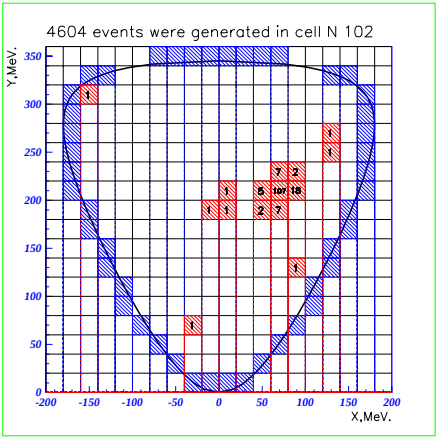

Figure 21: The spread of events initially simulated in the bin (70,210).

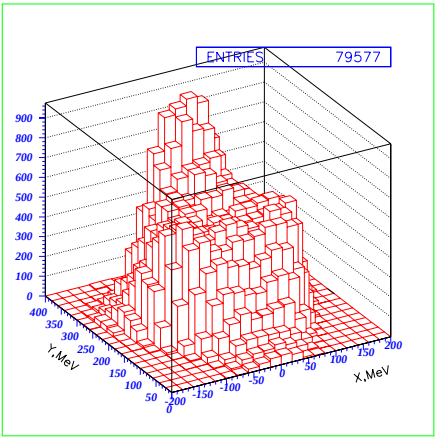

Figure 22: Dalitz distribution of experimental events.

The distribution of experimental 3π events is shown in Fig.22.

To approximate it we minimize the χ^2 functional of the form:

$$\chi^2 = \sum_{i=1}^{198} \frac{(N_i^{exp} - N_i^{calc})^2}{N_i^{exp} + \sigma_i^2(N^{calc})}, \tag{45}$$

N_i^{exp} – experimental number of events, $N_i^{calc}, \sigma_i(N^{calc})$ – calculated number of events and its error.

Free parameters of the fit are: N_0, a and φ.

Fig.23 shows cuts along Y axis for different X values of experimental Dalitz distribution (points) and fit result (histograms).

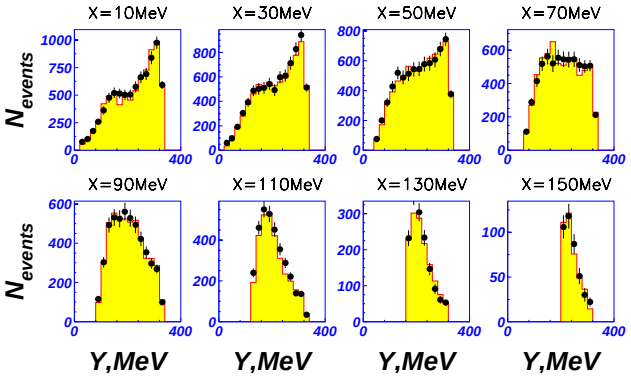

Figure 23: Result of the fit. Slices of the Dalitz distribution (right half) along Y axis for different values of X are shown. Points are experimental data, histogram – calculated numbers.

Obtained optimal parameters are given in Table 8. Also shown are the results on the value of the contact term found by KLOE[1] [12], SND [7],CMD-2 [6] groups.

Table 8: Results on absolute value and phase of contact amplitude

CMD-2 this work	$a = 0.101 \pm 0.044_{stat} \pm 0.017_{sys}$ $\varphi = -2.91 \pm 0.14_{stat} \pm 0.07_{sys}$ $\chi^2/N_{df} = 0.95$ significance 3.3σ
KLOE (2003)	$a = 0.104 \pm 0.010_{stat} \pm 0.020_{sys}$ $\varphi = -2.47 \pm 0.08_{stat} \pm 0.08_{sys}$
SND (2002)	$-0.06 < a < 0.06$ $\varphi = 0$-fixed; 90% CL
CMD-2 (1998)	$-0.15 < a < 0.10$ $\varphi = 0$-fixed; 90% CL

[1]In [12], p.8 $A_{dir} = a_d e^{i\phi_d}$ should be read as $A_{dir} = a_d e^{-i\phi_d}$ - private communication of the corresponding author Dr.C.Bini.

The systematic uncertainties come from nonuniformity of detection efficiency over the Dalitz plot, the uncertainty in the ρ-meson parameters and the model uncertainty in description of ρ-meson.

To take into account the nonuniformity of detection efficiency over the Dalitz plot we determine the total efficiency correction (see Sect.4) for several regions of π^+, π^- and π^0 momenta. This correction was applied to the Dalitz distribution. Difference between optimal parameters obtained in approximation with and without correction was taken as evaluation of considered systematic uncertainty, it was found to be 0.017 for a and 0.07 for φ.

The uncertainty in the ρ-meson parameters induces 2.6% systematic error for a and 1% error for φ. It was found varying ρ-meson mass $M_\rho = 775.8 \pm 0.5$ MeV/c^2 and width $\Gamma_\rho = 150.3 \pm 1.6$ MeV withing their PDG errors [17].

The model uncertainty was evaluated applying two different parametrizations of ρ-meson shape - relativistic Breit-Wigner and Gounaris-Sakurai formula [21]. This difference was found to be negligible.

The total systematic uncertainty was obtained by adding all the contributions in quadrature.

Good agreement between CMD-2 and KLOE result can be seen from Table 8. KLOE analysis is based on the 25 times larger data sample ($N_{3\pi}(KLOE) \approx 2000000$ [12]) of 3π events, so its statistical error is significantly smaller, however, KLOE and CMD-2 systematic uncertainties are the same.

The determined value of non-$\rho\pi$ amplitude is in agreement with theoretical estimations of the contact term [8], [9].

However, the higher resonances like $\rho(1450)$ or $\rho(1700)$ can contribute to the non-$\rho\pi$ term as well.

In assumption that the non-$\rho\pi$ amplitude is dominated by $\rho(1450)\pi(\rho'\pi)$ mechnism the theoretical number of events in the bin number k of Dalitz diagram is given by expression (similar to the Eq.39):

$$N_k^{th} = \frac{N_0}{Z}\int_k dXdY|\vec{P_+} \times \vec{P_-}|^2|A_{\rho'\pi}a'e^{i\varphi'} + A_{\rho\pi}|^2, \qquad (46)$$

where $A_{\rho'\pi}a'e^{i\varphi'}$ term stands instead of the contact amplitude and describes the $\rho'\pi$ contribution.

$$A_{\rho'\pi} = \frac{1}{D_{\rho'^+}(Q_+^2)} + \frac{1}{D_{\rho'^-}(Q_-^2)} + \frac{1}{D_{\rho'^0}(Q_0^2)}, \qquad (47)$$

where $\frac{1}{D_{\rho'^i}(Q_i^2)}$ is ρ'^i-meson ($i = +, -, 0$) propagator determined by the equation similar to the Eq.42. Parameters of the $\rho(1450)$ were taken from [17]:

$M_{\rho'} = 1465 \pm 25$ MeV/c^2 and $\Gamma_{\rho'} = 400 \pm 60$ MeV.

The admixture of the $A_{\rho,\pi}$ is described by the complex constant $a'e^{i\varphi'}$, its absolute value is related to the hadronic coupling constants according to equation:

$$a' = \frac{g_{\phi\rho'\pi} g_{\rho'\pi\pi}}{g_{\phi\rho\pi} g_{\rho\pi\pi}} \,. \tag{48}$$

Free parameters of the fit were: the total number of produced 3π events- N_0, a' and φ'. The obtained values are:

$$a' = 0.215 \pm 0.092 \pm 0.036,$$
$$\varphi' = 0.177 \pm 0.132 \pm 0.051,$$

where the first error is statistical and the second is systematical one, determined primarily by the uncertainty due to the nonuniformity of efficiency correction over the Dalitz diagram.

The $\frac{g_{\rho'\gamma} g_{\rho'\pi\pi}}{g_{\rho\gamma} g_{\rho\pi\pi}}$ ratio can be obtained from the study of $e^+e^- \to \pi^+\pi^-$ process around ρ-meson [20]:

$$\frac{g_{\rho'\gamma} g_{\rho'\pi\pi}}{g_{\rho\gamma} g_{\rho\pi\pi}} = -0.269 \pm 0.022, \tag{49}$$

Combining Eq.48 with $\frac{g_{\rho'\gamma} g_{\rho'\pi\pi}}{g_{\rho\gamma} g_{\rho\pi\pi}}$, the following ratio can be determined:

$$\frac{g_{\phi\rho'\pi}}{g_{\phi\rho\pi}} \Big/ \frac{g_{\rho'\gamma}}{g_{\rho\gamma}} = a' \Big/ \frac{g_{\rho'\gamma} g_{\rho'\pi\pi}}{g_{\rho\gamma} g_{\rho\pi\pi}}, \tag{50}$$

it was found to be:

$$\frac{g_{\phi\rho'\pi}}{g_{\phi\rho\pi}} \Big/ \frac{g_{\rho'\gamma}}{g_{\rho\gamma}} = -0.80 \pm 0.37 \,.$$

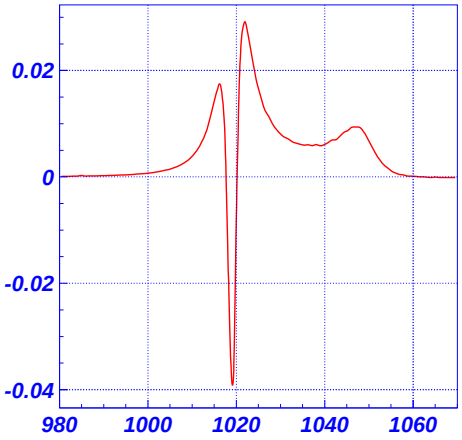

Figure 24: Beam energy spread correction δ_{wid} versus c.m. energy.

8 Appendix

A Correction for the beam energy spread

If relative cross section change $\Delta\sigma/\sigma$ over the energy scale of σ_E (RMS of the beam energy distribution) is large then visible cross section shape is essentially distorted in comparison with the physical one. In general the smeared cross section is given by equation:

$$\sigma_{smeared}(W) = \int \sigma(W') \frac{1}{\sqrt{2\pi}\Delta W} e^{-\frac{(W'-W)^2}{2\Delta W^2}} dW', \; W = 2E = \sqrt{s}, \qquad (51)$$

where $\sigma(W')$ is physical cross section at W' c.m. energy, W and ΔW (at VEPP-2M $\Delta W = \sqrt{2} \cdot 300 \simeq 420$ KeV) are mean value and RMS of the c.m. energy distribution.

Assuming that the correction is small one may decompose $\sigma(W')$ near the central value W:

$$\sigma(W') = \sigma(W) + \sigma'(W)(W' - W) + \frac{1}{2}\sigma''(W)(W' - W)^2 + ... \qquad (52)$$

and substitute it to Eq.51:

$$\sigma_{smeared}(W) = \sigma(W)(1 + \frac{\sigma''(W)\Delta W^2}{2\sigma(W)}) = \sigma(W)(1 + \delta_{wid}(W)) \qquad (53)$$

$\delta_{wid}(W)$ is the largest in the region were $\sigma''(W)$ is maximal i.e. on the ϕ-meson peak. Here its value is only few percent as shown in Fig.24.

B Logarithmic Gaussian function

This function is determined by the formula:

$$f_{LG}(x) = exp(-\frac{ln^2(1-\eta(x-x_0)/\sigma)}{2\sigma_0^2} - \frac{\sigma_0^2}{2})\frac{\eta}{\sqrt{2\pi}\sigma\sigma_0}, \qquad (54)$$

where: x_0 – peak position, η – assymetry, σ – width, $\sigma_0 = \frac{2}{\xi}arcsh(\frac{\eta\xi}{2})$, $\xi = 2\sqrt{2ln2} \approx 2.35$.

Acknowledgments.

The authors are grateful to the staff of VEPP-2M for the excellent performance of the collider, to all engineers and technicians who participated in the design, commissioning and operation of CMD-2.

References

[1] *G.A. Aksenov et al.* Preprint Budker INP 85-118, Novosibirsk, 1985.

[2] *E.V. Anashkin et al.* ICFA Inst. Bull., **5** (1988) 18.

[3] *V.V. Anashin et al.* Preprint Budker INP 84-114, Novosibirsk, 1984.

[4] *M. Gell-Mann, D. Sharp, W.G. Wagner.* Phys. Rev. Lett., **8**, 261 (1962).

[5] *G. Parrour et al.* Phys. Lett. B, **63**, 362 (1976).

[6] *R.R. Akhmetshin et al.* Phys. Lett. B, **434**, 426 (1998).

[7] *M.N. Achasov et al.* Phys. Rev. D, **65**, 032002 (2002).

[8] *Y. Brihaye, N.K. Pak, P. Rossi.* Nucl. Phys. B, **254**, 71 (1985).

[9] *O. Kaymakcalan, S. Rajeev, J. Schechter.* Phys. Rev. D, **30**, 594 (1984).

[10] *E.A. Kuraev, Z.K. Silagadze.* Phys. Atom. Nucl., **58**, 1589 (1995).

[11] *T. Fujiwara et al.* Progress of Theoretical Physics, **73**, 926 (1985).

[12] *A. Aloisio et al.* Phys. Lett. B, **561**, 55 (2003).

[13] *D. Epifanov.* Proc. of the International Conference: "DAΦ NE 2004 PHYSICS AT MESON FACTORIES", Frascati, June 2004, p.389.

[14] *K.Y. Mikhailov.* Master thesis, Novosibirsk, 1998.

[15] *R. Brun et al.* GEANT - detector description and simulation tool, Geneva, 1994.

[16] *E.A. Kuraev, V.S. Fadin.* Sov. J. of Nucl. Phys., **41**, 466 (1985).

[17] *S. Eidelman et al.* Phys. Lett. B, **592**, 1 (2004).

[18] *M.N. Achasov et al.* Phys. Rev. D, **63**, 072002 (2001).

[19] *B. Aubert et al.* Phys. Rev. D, **70**, 072004 (2004).

[20] *R.R. Akhmetshin et al.* Phys. Lett. B, **527**, 161 (2002).

[21] *G.J. Gounaris, J.J. Sakurai.* Phys. Rev. Lett., **21**, 244 (1968).

Contents

R.R. Akhmetshin, V.M. Aulchenko, V.Sh. Banzarov, L.M. Barkov,
N.S. Bashtovoy, A.E. Bondar, D.V. Bondarev, A.V. Bragin,
S.K. Dhawan, S.I. Eidelman, D.A. Epifanov, G.V. Fedotovich,
N.I. Gabyshev, D.A. Gorbachev, A.A. Grebeniuk, D.N. Grigoriev,
F.V. Ignatov, S.V. Karpov, V.F. Kazanin, B.I. Khazin,
I.A. Koop, P.P. Krokovny, A.S. Kuzmin, I.B. Logashenko,
P.A. Lukin, A.P. Lysenko, K.Yu. Mikhailov, A.I. Milstein,
I. N. Nesterenko, M.A. Nikulin, V.S. Okhapkin, A.V. Otboev,
E.A. Perevedentsev, A.A. Polunin, A.S. Popov, S.I. Redin,
B.L. Roberts, N.I. Root, A.A. Ruban, N.M. Ryskulov,
A.G. Shamov, Yu.M. Shatunov, B.A. Shwartz, A.L. Sibidanov,
V.A. Sidorov, A.N. Skrinsky, V.P. Smakhtin, I.G. Snopkov,
E.P. Solodov, A.A. Valishev, Yu.V. Yudin, A.S. Zaitsev,
S.G. Zverev

CMD-2 Collaboration

Study of $\phi \to \pi^+\pi^-\pi^0$ with CMD-2 detector

Р.Р. Ахметшин и др.

Изучение распада $\phi \to \pi^+\pi^-\pi^0$ с детектором КМД-2

Budker INP 2006-28

Ответственный за выпуск А.М. Кудрявцев
Работа поступила 19.05.2006 г.

Сдано в набор 22.05.2006 г.
Подписано в печать 23.05. 2006 г.
Формат бумаги 60×90 1/16 Объем 2.5 печ.л., 2.2 уч.-изд.л.
Тираж 120 экз. Бесплатно. Заказ № 28

Обработано на IBM PC и отпечатано на
ротапринте "ИЯФ им. Г.И. Будкера" СО РАН
Новосибирск, 630090, пр. академика Лаврентьева, 11.